A Methodology for Modeling and Simulating Frictional Translational Joint with a Flexible Slider and Clearance in Multibody Systems

Xudong Zheng[1], Qi Wang[2]

School of Aeronautic Science and Engineering, Beihang University
[1] *xudongzheng_buaa@163.com;* [2] *bhwangqi@sina.com*

ABSTRACT —*The objective of this paper is to present a simple and effective methodology for modeling and simulating planar multibody systems including frictional translational joint with a flexible slider and clearance. By using the finite element method (FEM), the slider is divided into finite elements, and the distributed body forces and boundary stresses (contact forces) on the slider are equivalent to the nodal forces. The normal contact forces are modeled by virtual spring-dampers, while the frictional forces are described by the Coulomb dry friction model. By lumping the mass matrix and presenting it in diagonal form, the equations of motion are then inertially decoupled, and the frictional forces are solved independently via trial-and-error algorithm. A penalty method for the revolute joint connecting the slider and other bodies is applied, and equations of motion are integrated numerically. Finally, two numerical examples are given to test the feasibility and effectiveness of the methodology in this paper.*

1 Introduction

Over the last decades, researchers have conducted a lot of studies considering multibody mechanical systems with imperfect joints [1-18], and reviews were made in this field [19,20]. As a branch of this area, modeling and simulating translational joints with clearances in multibody systems have attracted the attention of many authors. Wilson et al. [21], Farahanchi et al. [22], and Klepp [23] were the pioneers in studying mechanism dynamics with imperfect translational joints. In recent years, Qi et al. [24] presented a frictional contact analysis for multibody systems with spatial prismatic joints on the basis of tiny clearances. Flores et al. [25,26] proposed a methodology for dynamic modeling and analysis of rigid multibody systems with translational clearance joints using the nonsmooth dynamics approach. In their study, the resulting contact-impact problem was formulated and solved as a linear complementarity problem (LCP) [27-29], which was embedded in the Moreau time-stepping method. Flores [26] demonstrated that some numerical difficulties can arise when the clearance size is very small, which lead to drift problem. Acary et al. [30,31] investigated the numerical time-integration algorithms for nonsmooth mechanical systems subjected to unilateral contacts, impacts and Coulomb's friction, and verified their algorithms by comparing with Flores' study [26]. To overcome the drift problem, Zhuang et al. [32,33] combined Baumgarte's stabilization method with horizontal linear complementarity problem (HLCP) approach for dynamic modeling and simulating of frictional translational joints with tiny clearances in rigid multibody systems. Using Ting's rotatability laws, Ting et al. [34] presented a novel kinematic model to quantify the effects of the joint clearance on the output position uncertainty of any single loop linkage containing revolute or prismatic joints. All these above-mentioned studies about imperfect translational joints were based on rigid slider models, and the influence of the slider deformation was not studied. In view of this, Zhang et al. [35] analyzed the deformation of the slider and the clearance size using KED technique and penalty method. However, tedious judgements of the contact

states between the slider and its guide were introduced in their study. What's more, the KED technique ignored the coupling between rigid body and flexible body motion [36].

The purpose of this study is to present a simple and effective methodology for modeling and simulating frictional translational joint with a flexible slider and clearance in multibody systems. The reminder of this paper is organized as follows. In Section 2, the FEM discretization of the slider, normal and tangential contact forces, as well as penalty method for the revolute joint are introduced. In Section 3, Equations of motion of the system are established, and computer procedures for dynamic analysis are given. In Section 4, two demonstrative examples are presented, and the results are compared with previous studies. Finally, in the last section, the main conclusions from this study are drawn.

2 FEM discretization of the slider and contact forces

2.1 FEM discretization of the slider

As shown in Fig. 1, a translational joint often consists of the guide, a slider, and a revolute joint. For simplicity, the guide is fixed on the ground, i.e., the slider only has translational motion. An inertial frame of reference *Oxy* is established on the ground. The slider is treated as flexible in this study. By using the FEM technique, the slider is divided into a finite number of elements, and the distributed body forces and boundary stresses (normal and tangential contact forces) on the slider are equivalent to the nodal forces. The nodes are labeled as illustrated in Fig. 1, and each node has two degrees of freedom. The revolute joint is considered as perfect, that is to say, there is no clearance and friction in the revolute joint. The revolute joint connects the slider with other bodies via the node n_R.

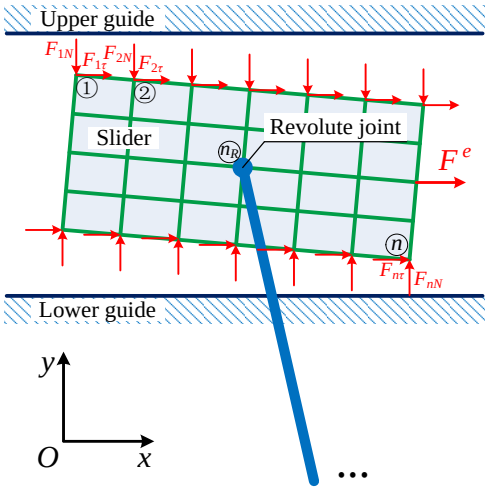

Fig. 1: The FEM discretization of the slider

2.2 Normal contact forces

In this paper, as shown in Fig. 2, the surfaces of the guide are modeled by appending plenty of virtual spring-dampers in the normal directions [37]. The spring-dampers work only if the surface nodes are in contact with or penetrate the guide surfaces, and the normal contact forces can never be negative [38]. The normal contact force acting at node *i* is expressed as

$$F_{iN} = \begin{cases} \max\{K\delta_i + \chi\dot{\delta}_i,\ 0\}, & \delta_i \geq 0 \\ 0, & \delta_i < 0 \end{cases} \tag{1}$$

where F_{iN} is the normal contact force. δ_i and $\dot{\delta}_i$ are the penetration depth and penetration velocity of node *i*, respectively. K is the generalized stiffness parameter, while χ is the hysteresis factor.

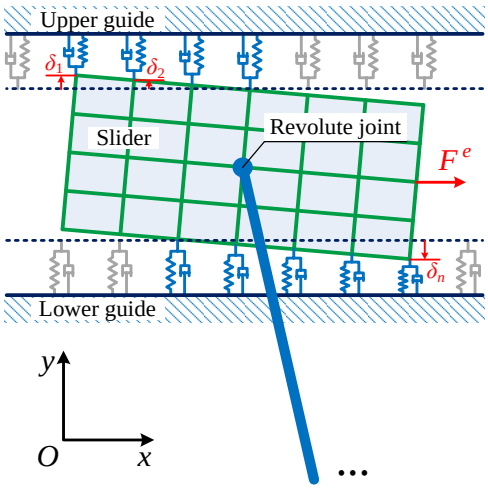

Fig. 2: The normal contact forces

2.3 Tangential contact forces

The Coulomb dry friction model has been employed by many researchers in the field of modeling and simulating non-smooth multibody systems [25,32,35,39,40]. This model has the superiority to simulate stiction and to capture stick-slip motion. It has been demonstrated that the Coulomb dry friction model requires less computational time and fewer selected parameters than the bristle-based friction models [5,41]. What's more, the Coulomb friction coefficients can be easily obtained by experiments or by consulting handbooks on friction. Therefore, the Coulomb dry friction model is adopted to evaluate the tangential contact forces in this paper.

The Coulomb dry friction model can be expressed as

$$F_{i\tau}=\begin{cases}-\mu F_{iN}\,\mathrm{sgn}\left(v_{i\tau}\right), & v_{i\tau}\neq 0\\ -\mu' F_{iN}\mathrm{Sgn}\left(a_{i\tau}\right), & v_{i\tau}=0\end{cases} \tag{2}$$

where $F_{i\tau}$ is the tangential contact force acting at node *i*. μ is the coefficient of kinetic friction, while μ' is that of static friction, and μ is usually smaller than μ'. $v_{i\tau}$ is the tangential velocity (component of velocity in *x* direction) of node *i*, and $a_{i\tau}=\mathrm{d}v_{i\tau}/\mathrm{d}t$. $\mathrm{sgn}(x)$ is the sign function, while $\mathrm{Sgn}\left(x\right)$ is the multivalued function, which is defined as [42],

$$\mathrm{Sgn}\left(x\right)=\begin{cases}+1, & x>0\\ [-1,+1], & x=0\\ -1, & x<0\end{cases} \tag{3}$$

The Coulomb dry friction model is illustrated in Fig. 3.

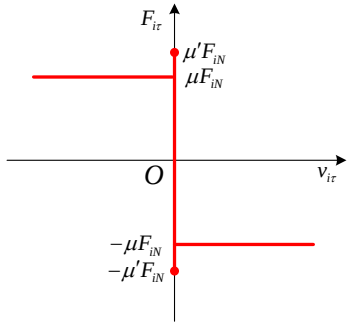

Fig. 3: The Coulomb dry friction model

2.4 Penalty method for the revolute joint

There are two common techniques dealing with the perfect revolute joint. One is the famous Lagrange multipliers method, the other is the penalty method [43], which is equivalent to two springs acting at the pin of the joint, as illustrated in Fig. 4. The penalty method is easy to implement as compared to the Lagrange multipliers method, which introduces the differential-algebraic equations that are difficult to solve. Therefore, the penalty method is applied for the perfect revolute joint in this study. The forces from the revolute joint acting at the node n_R are evaluated as

$$\begin{cases} F_{RX} = k_{RX}\left(x_R - x_{n_R}\right) \\ F_{RY} = k_{RY}\left(y_R - y_{n_R}\right) \end{cases} \tag{4}$$

where F_{RX} and F_{RY} are two forces from the revolute joint. x_R and y_R are the components of the position vector of the revolute joint, while x_{n_R} and y_{n_R} are that of the node n_R. k_{RX} and k_{RY} are the penalty factors.

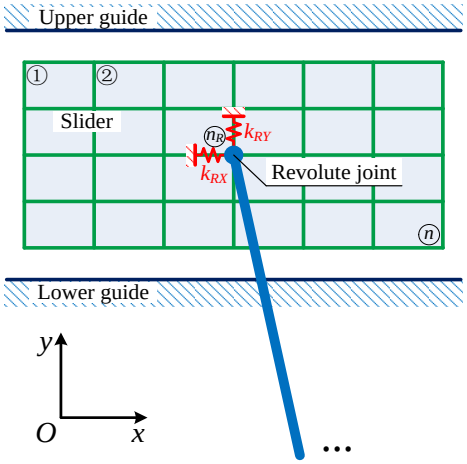

Fig. 4: Penalty method for the revolute joint

3 Equations of motion of the system and computer procedures

3.1 Equations of motion of the system

As the slider only has translational motion, its equations of motion can be written as

$$\boldsymbol{M}\ddot{\boldsymbol{u}} + \boldsymbol{C}\dot{\boldsymbol{u}} + \boldsymbol{K}\boldsymbol{u} = \tilde{\boldsymbol{Q}} + \boldsymbol{Q}_N + \boldsymbol{Q}_\tau + \boldsymbol{Q}_{F_R} \tag{5}$$

where $\boldsymbol{M}$, $\boldsymbol{C}$, and $\boldsymbol{K}$ are mass, damping, and stiffness matrices of the slider, respectively. $\boldsymbol{u}$, $\dot{\boldsymbol{u}}$, and $\ddot{\boldsymbol{u}}$ are the vectors of displacements, velocities, and accelerations of the nodes, respectively. $\boldsymbol{Q}_N$ is the equivalent nodal forces vector of normal contact forces, while $\boldsymbol{Q}_\tau$ is that of tangential contact forces. $\boldsymbol{Q}_{F_R}$ contains the forces from the revolute joint, and $\tilde{\boldsymbol{Q}}$ is the equivalent nodal forces vector of other forces such as gravity and externally applied forces.

The Rayleigh damping matrix is used in this paper

$$\boldsymbol{C} = \alpha\boldsymbol{M} + \beta\boldsymbol{K} \tag{6}$$

where the parameters α and β are determined experimentally [44].

Other bodies of the system are treated as rigid, thus, their equations of motion are

$$\ddot{\boldsymbol{q}} = \boldsymbol{f}\left(t, \boldsymbol{q}, \dot{\boldsymbol{q}}, \boldsymbol{F}_R\right) \tag{7}$$

where $\boldsymbol{q}$, $\dot{\boldsymbol{q}}$, and $\ddot{\boldsymbol{q}}$ are the vectors of generalized coordinates, velocities, and accelerations of other bodies, respectively. $\boldsymbol{F}_R$ contains the forces from the revolute joint.

Combining Eqs.(5) and (7) yields the equations of motion of the system

$$\begin{cases} \boldsymbol{M}\ddot{\boldsymbol{u}} + \boldsymbol{C}\dot{\boldsymbol{u}} + \boldsymbol{K}\boldsymbol{u} = \tilde{\boldsymbol{Q}} + \boldsymbol{Q}_N + \boldsymbol{Q}_\tau + \boldsymbol{Q}_{F_R} \\ \ddot{\boldsymbol{q}} = \boldsymbol{f}\left(t, \boldsymbol{q}, \dot{\boldsymbol{q}}, \boldsymbol{F}_R\right) \end{cases} \tag{8}$$

3.2 Computer procedures for dynamic analysis of the system

In order to integrate the differential equations of motion (8) numerically, the vector $\boldsymbol{Q}_\tau$ needs to be calculated first. By lumping the mass matrix $\boldsymbol{M}$ and presenting it in diagonal form, Eq.(5) is then inertially decoupled [44]. Therefore, the frictional forces acting at the surface nodes can be solved independently of each other via trial-and-error algorithm. On some occasions such lumping is physically obvious, in others this is not the case and a rational procedure is required. As Eq.(5) is inertially decoupled, the equations of motion of the surface node *i* can be written as

$$\begin{cases} m_{2i-1}\ddot{u}_{2i-1} + \sum_j c_{2i-1,j}\dot{u}_j + \sum_j k_{2i-1,j}u_j = \tilde{Q}_{2i-1} + Q^N_{2i-1} + Q^\tau_{2i-1} + Q^{F_R}_{2i-1} \\ m_{2i}\ddot{u}_{2i} + \sum_j c_{2i,j}\dot{u}_j + \sum_j k_{2i,j}u_j = \tilde{Q}_{2i} + Q^N_{2i} + Q^\tau_{2i} + Q^{F_R}_{2i} \end{cases} \tag{9}$$

which are the rows 2*i*-1 and 2*i* of Eq.(5)

Thus,

$$\begin{bmatrix} Q^N_{2i-1} \\ Q^N_{2i} \end{bmatrix} = \begin{bmatrix} 0 \\ -F_{iN} \end{bmatrix} \text{ (for the upper surface)} \tag{10}$$

or

$$\begin{bmatrix} Q^N_{2i-1} \\ Q^N_{2i} \end{bmatrix} = \begin{bmatrix} 0 \\ F_{iN} \end{bmatrix} \text{ (for the lower surface)} \tag{11}$$

and

$$\begin{bmatrix} Q^\tau_{2i-1} \\ Q^\tau_{2i} \end{bmatrix} = \begin{bmatrix} F_{i\tau} \\ 0 \end{bmatrix} \tag{12}$$

What's more, $v_{i\tau} = \dot{u}_{2i-1}$ and $a_{i\tau} = \ddot{u}_{2i-1}$.

Therefore, the trial-and-error algorithm for the frictional force $F_{i\tau}$ acting at the surface node *i* is expressed as

$$\begin{aligned} &\text{if } (v_{i\tau} \neq 0) \\ &\quad F_{i\tau} = -\mu F_{iN}\,\mathrm{sgn}\left(v_{i\tau}\right) \\ &\text{else} \\ &\quad F_{i\tau} = \sum_j c_{2i-1,j}\dot{u}_j + \sum_j k_{2i-1,j}u_j - \tilde{Q}_{2i-1} - Q^{F_R}_{2i-1} \\ &\quad \text{if } (F_{i\tau} > \mu' F_{iN}) \quad F_{i\tau} := \mu' F_{iN} \\ &\quad \text{if } (F_{i\tau} < -\mu' F_{iN}) \quad F_{i\tau} := -\mu' F_{iN} \\ &\text{end if} \end{aligned} \tag{13}$$

In this study, when $v_{i\tau} \le \varepsilon = 1\times10^{-5}$ m/s, the tangential velocity of node *i* is treated as zero [45]. After obtaining the vector $\boldsymbol{Q}_\tau$, the equations of motion (8) can be integrated by a numerical method for ordinary differential equations. The computer procedures for multibody systems including frictional translational joint with a flexible slider and clearance is illustrated in Fig. 5.

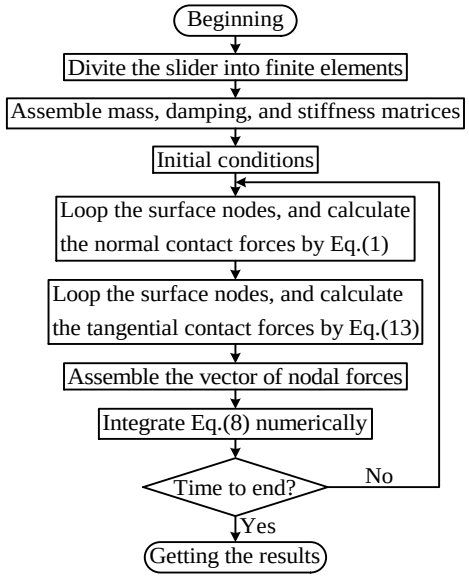

Fig. 5: Computer procedures for multibody systems including frictional translational joint with a flexible slider and clearance

4 Numerical examples

In order to test the applicability and correctness of the methodology proposed by this paper, two numerical examples are given, and the results are compared with previous studies. The first is a stick-slip oscillator [35], while the second is a planar slider-crank mechanism [32].

4.1 A stick-slip oscillator

The FEM discretization of a stick-slip oscillator is illustrated in Fig. 6. The slider is subjected to the applied force $F = F_{\max} \sin \Omega t$ and is attached to a spring of stiffness k. The uniform slider is divided into 25 four-node quadrilateral elements, and the parameters and initial conditions necessary to perform the dynamic analysis of the stick-slip oscillator are listed in Tab. 1.

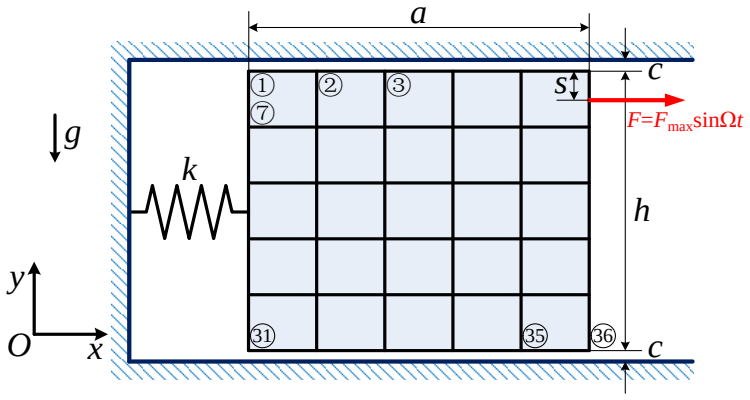

Fig. 6: FEM discretization of a stick-slip oscillator

Geometric characteristics	Width of slider	$a = 0.6$ m
	Height of slider	$h = 0.5$ m
	Clearance size	$c = 2.5$ mm
	Position of applied force	$s = 0.05$ m
	Density	$\rho = 1/3$ kg/m^2

Material properties	Young's modulus	$E = 1000$ Pa
	Poisson's ratio	$\upsilon = 0.3$
	Rayleigh parameters	$\alpha = 0.010,\ \beta = 0.544$
Contact parameters	Generalized stiffness parameter	$K = 1\times10^{4}$ N/m
	Hysteresis factor	$\chi = 1\times10^{3}$ N·s/m
	Coefficient of kinetic friction	$\mu = 0.15$
	Coefficient of static friction	$\mu' = 0.20$
External forces	Amplitude of applied force	$F_{\max} = 1.5$ N
	Angular frequency of applied force	$\Omega = \pi / 10$
	Spring stiffness	$k = 1.0$ N/s
	Gravitational acceleration	$g = 9.81$ m/s^2
Initial conditions	Vector of displacements	$\boldsymbol{u} = \boldsymbol{0}$
	Vector of velocities	$\dot{\boldsymbol{u}} = \boldsymbol{0}$

Tab. 1: Parameters and initial conditions of the stick-slip oscillator

Fig. 7(b) shows the velocities of four corner nodes (nodes 1, 6, 31, and 36) in *x* direction, and it indicates that the slider moves with stick-slip phenomena. The results agree with Reference [35] closely. The velocities of these four corner nodes in *y* direction are illustrated in Fig. 8. It shows that the components of velocities in *y* direction are much smaller than that in *x* direction. Velocities of nodes 1 and 6 in *y* direction always have opposite signs, and they quickly decrease to zero when the corresponding nodes impact with the upper guide.

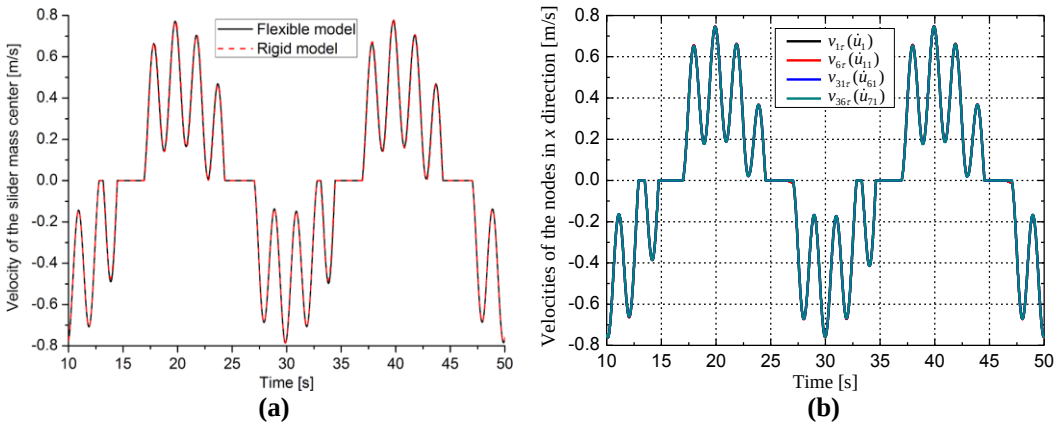

Fig. 7: Velocities in *x* direction: (a) Reference [35]; (b) this paper

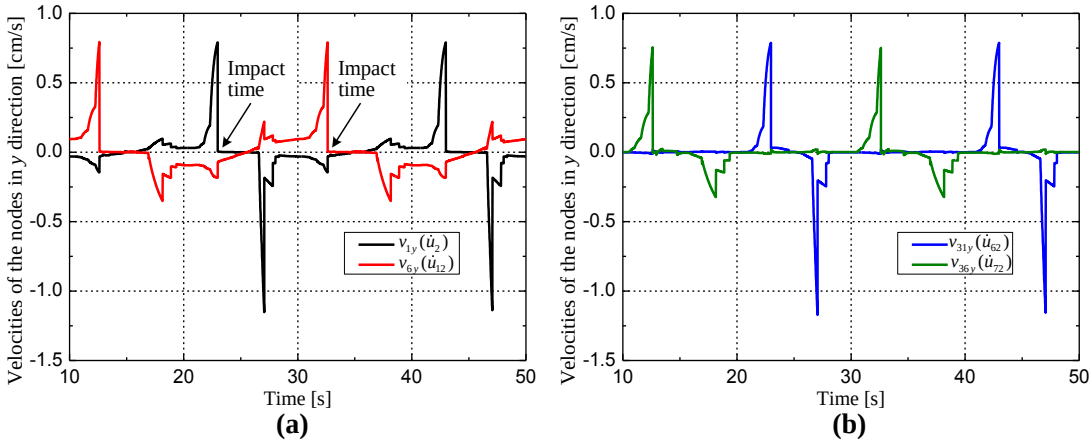

Fig. 8: Velocities of the nodes in *y* direction: (a) nodes 1 and 6; (b) nodes 31 and 36

Fig. 9 depicts the sum of frictional forces acting on the slider. The results of this paper are consistent with Reference [35] very well. As Young's modulus, clearance size, as well as numerical methods adopted in this paper are different from Reference [35], the results are not identical. The frictional forces acting at the surface nodes are illustrated in Fig. 10. It shows that the frictional forces acting at nodes 2, 3, 4, and 5 are always zero, which means that these nodes are never in contact with the guide.

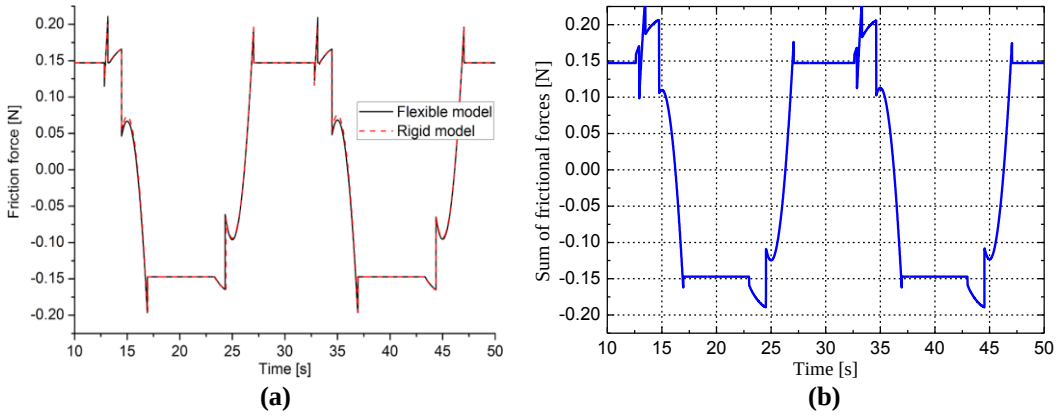

Fig. 9: Sum of frictional forces on the slider: (a) Reference [35]; (b) this paper

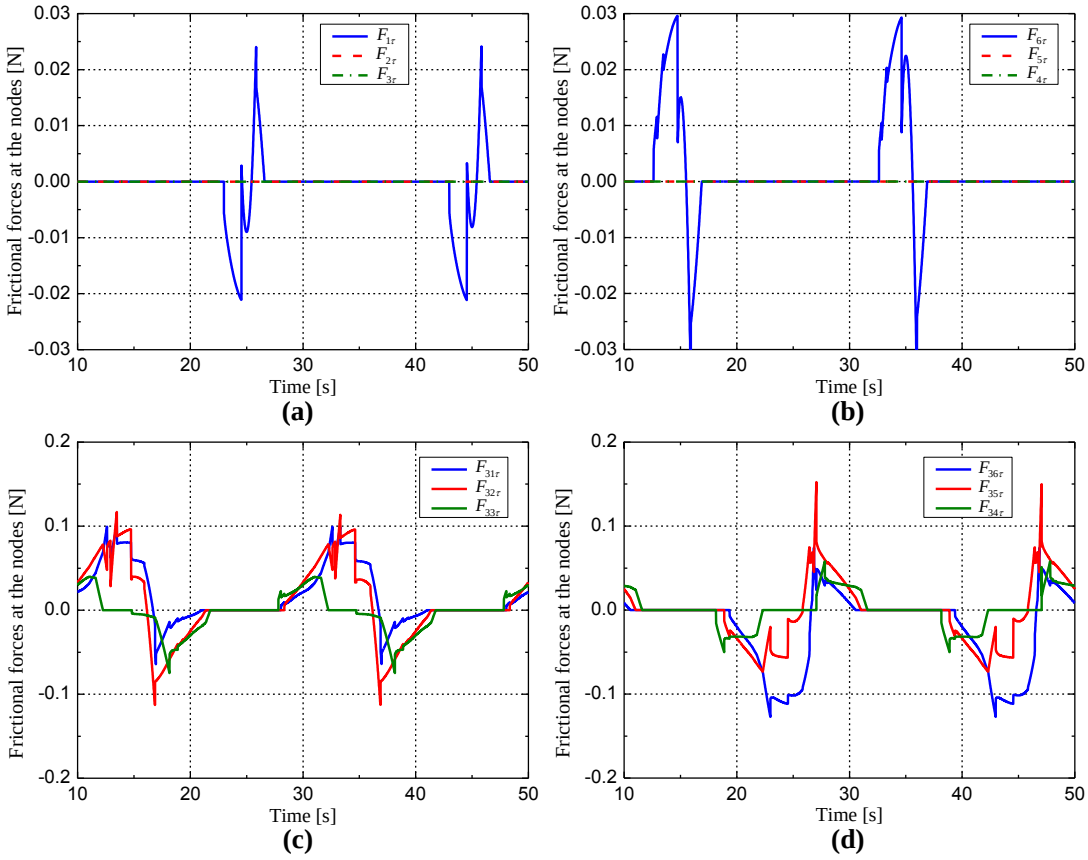

Fig. 10: Frictional forces at the nodes: (a) nodes 1, 2, and 3; (b) nodes 4, 5, and 6; (c) nodes 31, 32, and 33; (d) nodes 34, 35, and 36

Fig. 11 illustrates the normal and tangential contact forces acting at the four corner nodes and average tangential velocities of these nodes $\bar{v}_\tau$, and $\bar{v}_\tau = \frac{1}{4}\left(v_{1\tau} + v_{6\tau} + v_{31\tau} + v_{36\tau}\right)$. The solid lines in Fig. 11(a) are normal contact forces at the left corner nodes (nodes 1 and 31), which show that these values are subjected to the complementarity conditions [32]:

$$F_{1N} \geq 0,\ F_{31N} \geq 0,\ F_{1N} \cdot F_{31N} = 0$$

Similarly, as shown in the dashed lines, the normal contact forces at the right corner nodes (nodes 6 and 36) are subjected to

$$F_{6N} \geq 0,\ F_{36N} \geq 0,\ F_{6N} \cdot F_{36N} = 0$$

It should be highlighted that when two opposite corners of a rigid slider touch the guide with zero tangential velocities, a well-known statically indeterminate problem will arise. Therefore, the values of frictional forces at the corners cannot be calculated exactly for the rigid model in these situations. These problems can be solved by considering the deformation of the slider, as depicted in Fig. 11(b).

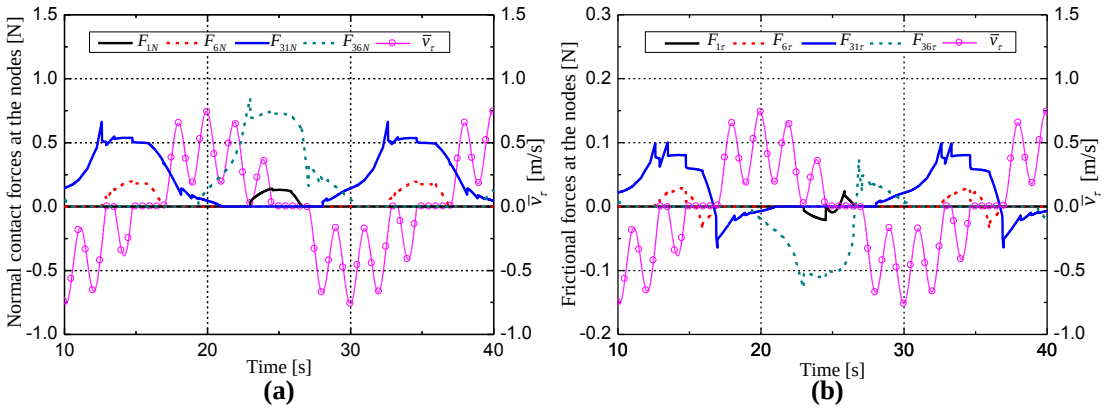

Fig. 11: Normal and frictional forces at nodes 1, 6, 31, and 36 and average tangential velocities of the nodes: (a) Normal contact forces; (b) frictional forces

4.2 A planar slider-crank mechanism

A planar slider-crank mechanism including frictional translational joint with a flexible slider and clearance is shown in Fig. 12. In this system, the crank and the connecting rod are uniform rigid rods, and all revolute joints are perfect. The driving crank moment is $P = P_0 \sin \Omega t$. The parameters and initial conditions used in the simulation are listed in Tab. 2.

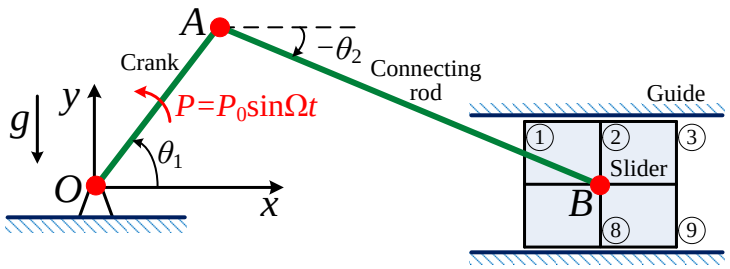

Fig. 12: Slider-crank mechanism with a frictional translational joint

Geometric characteristics	Length of crank *OA*	$L_1 = 1.8$ m
	Length of connecting rod *AB*	$L_2 = 2.0$ m
	Width of slider	$a = 0.5$ m
	Height of slider	$h = 0.3$ m
	Clearance size	$c = 2.5$ mm
Material properties	Mass of crank *OA*	$m_1 = 2.0$ kg
	Mass of connecting rod *AB*	$m_2 = 1.0$ kg
	Density of slider	$\rho = 20/3$ kg/m^2
	Young's modulus of slider	$E = 1000$ Pa
	Poisson's ratio of slider	$\upsilon = 0.3$
	Rayleigh parameters of slider	$\alpha = 0.010,\ \beta = 0.544$
Contact parameters	Generalized stiffness parameter	$K = 1\times10^4$ N/m
	Hysteresis factor	$\chi = 1\times10^3$ N·s/m
	Coefficient of kinetic friction	$\mu = 0.03$
	Coefficient of static friction	$\mu' = 0.04$

	Penalty factors for revolute joint B	$k_{RX} = k_{RY} = 1\times10^5$ N/m
External forces	Amplitude of applied moment	$P_0 = 6.0$ Nm
	Angular frequency of applied moment	$\Omega = \pi / 6$
	Gravitational acceleration	$g = 9.81$ m/s^2
Initial conditions	Displacements vector of the slider	$\boldsymbol{u} = \boldsymbol{0}$
	Velocities vector of the slider	$\dot{\boldsymbol{u}} = \boldsymbol{0}$
	Generalized coordinates vector of other bodies	$\boldsymbol{q}_0 = \begin{bmatrix} \theta_{10} \\ \theta_{20} \end{bmatrix} = \begin{bmatrix} 0 \text{ rad} \\ 0 \text{ rad} \end{bmatrix}$
	Generalized velocities vector of other bodies	$\dot{\boldsymbol{q}}_0 = \begin{bmatrix} \dot{\theta}_{10} \\ \dot{\theta}_{20} \end{bmatrix} = \begin{bmatrix} 0 \text{ rad/s} \\ 0 \text{ rad/s} \end{bmatrix}$

Tab. 2: Parameters and initial conditions of the slider-crank mechanism

First, the uniform slider is divided into 4 four-node quadrilateral elements, and the connecting rod is connected with the slider through the centric node (node 5). The angular position and angular velocity of the crank are illustrated in Fig. 13. It can be seen that the crank shows a periodic stick-slip motion. The results generated in this work agree with Reference [32] very well. The occurrence of stick-slip motion relates to the angular frequency of the applied driving crank moment [32].

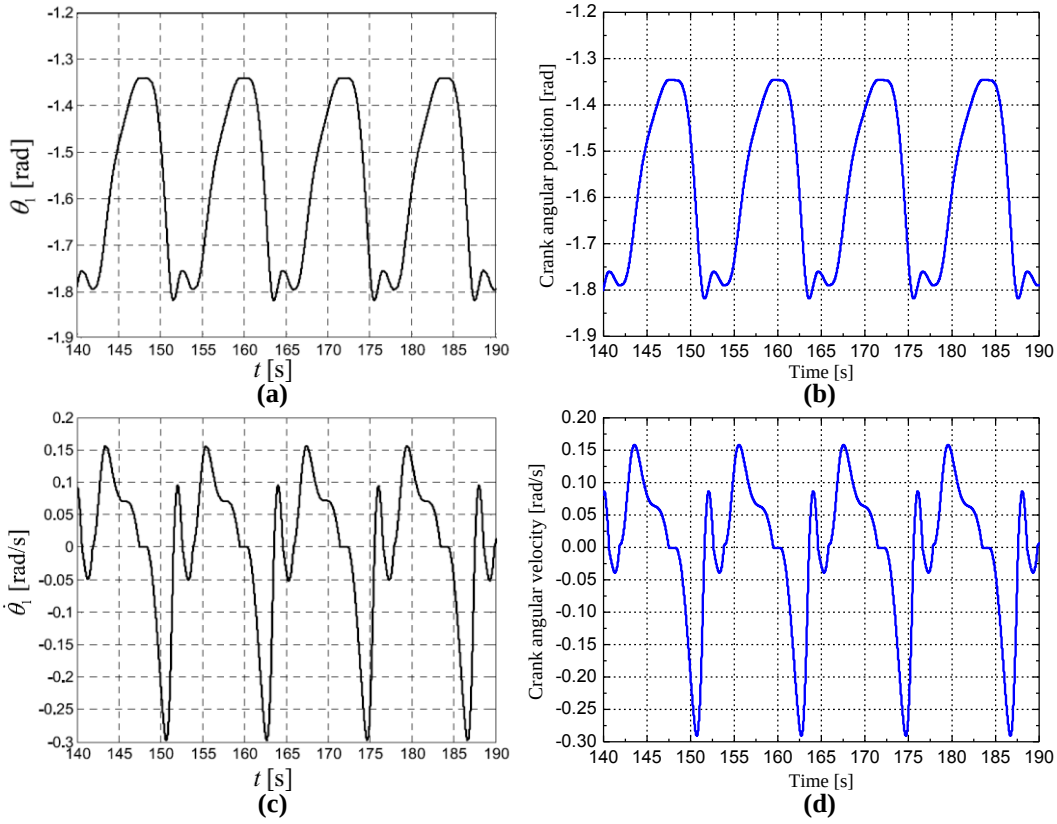

Fig. 13: Angular position and velocity of the crank: (a) and (c) Reference [4]; (b) and (d) this paper

Fig. 14 shows the sum of frictional forces acting on the slider. The results are consistent with Reference [32]. However, due to the flexibility of the slider, the maximum static frictional force yielded in this work is smaller

than that generated by a rigid model, as illustrated in the green circles. A more complex FEM discretization (8 four-node quadrilateral elements) of the slider is also made, and the results are shown in Fig. 14(b). Using more elements, the results will be more accurate, but more computation time will be expended also. In our study, to simulate 200 seconds, the elapsed CPU time for the 4 elements model is about 155 seconds, while for the 8 elements model is about 415 seconds (Intel Pentium 3.4 GHz). The 4 elements discretization of the slider can generate acceptable results, as depicted in Figs 13 and 14.

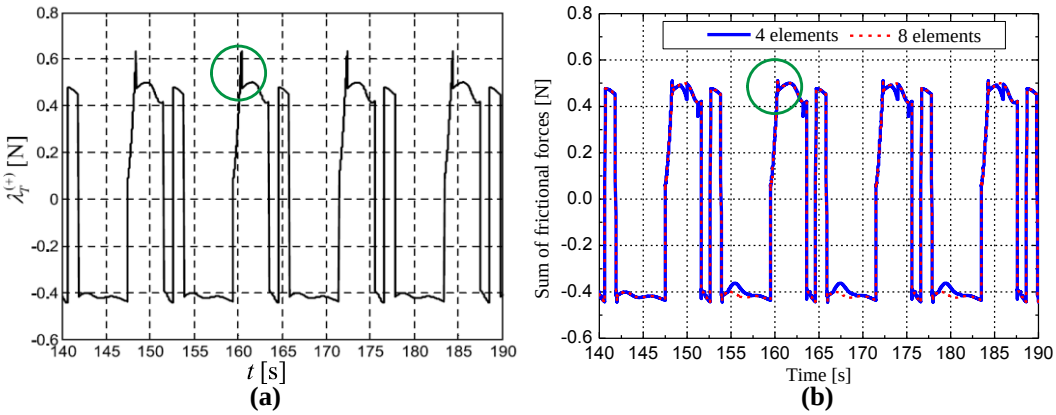

Fig. 14: Sum of frictional forces on the slider: (a) Reference [32]; (b) this paper

Figs. 15 and 16 illustrate the normal and tangential contact forces acting at the surface nodes for the 4 elements model, respectively. It reveals that when the motion is stable, only lower surface of the slider is in contact with the guide. In Fig. 16, the frictional forces acting at the nodes of lower surface have the mutation phenomena during the transitions of the nodes from stick to slip.

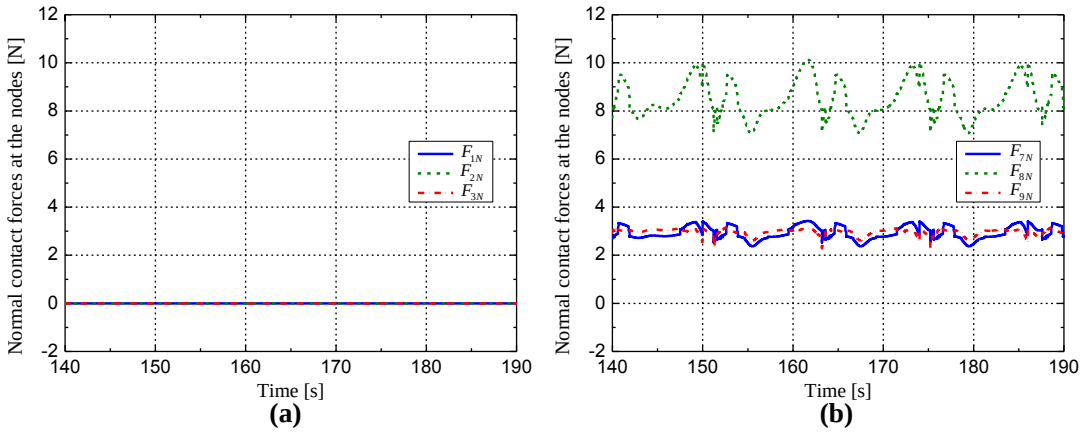

Fig. 15: Normal contact forces at the nodes: (a) nodes 1, 2, and 3; (b) nodes 7, 8, and 9

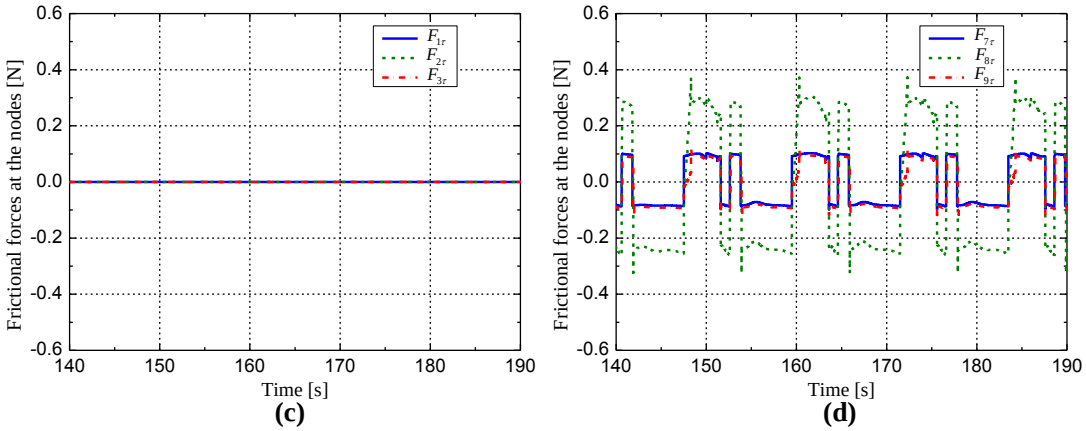

Fig. 16: Frictional forces at the nodes: (a) nodes 1, 2, and 3; (b) nodes 7, 8, and 9

Fig. 17 depicts the differences between position vector components: $x_R - x_5$ and $y_R - y_5$. As described in Section 2.4, x_R and y_R are the components of the position vector of the revolute joint B (one end of the connecting rod), while x_5 and y_5 are that of the node 5. It can be seen that these differences can remain bounded within 8×10^{-4} m on the basis of penalty method for the revolute joint.

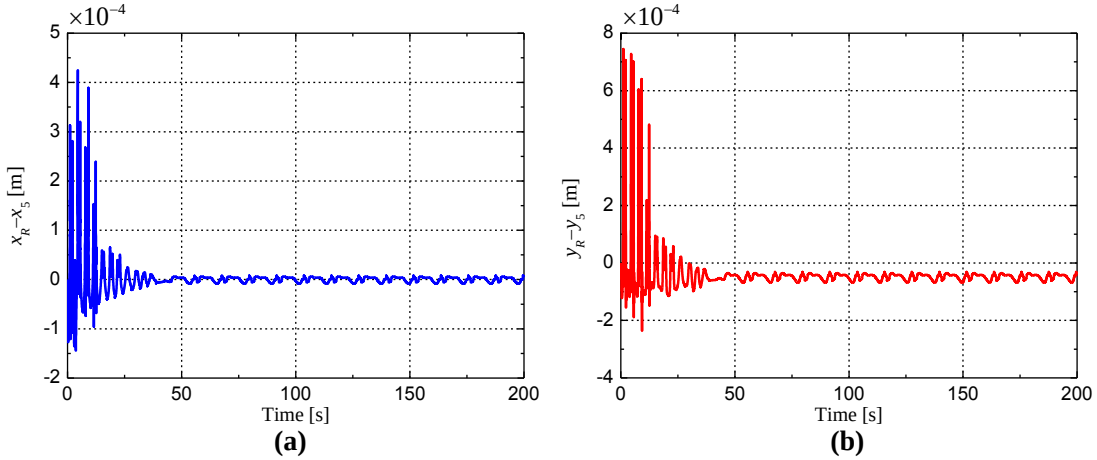

Fig. 17: Differences between position vector components: (a) $x_R - x_5$; (b) $y_R - y_5$

5 Conclusions

This paper presented a novel methodology for modeling and simulating multibody systems including frictional translational joint with a flexible slider and clearance. Firstly, the slider was divided into a finite number of elements based on FEM, and the distributed body forces and boundary stresses (normal and tangential contact forces) acting on the slider were equivalent to the nodal forces. Secondly, the normal contact forces were obtained by using the model of virtual spring-dampers, while the frictional forces were described by the Coulomb dry friction model. Thirdly, by lumping the mass matrix and presenting it in diagonal form, the equations of motion were inertially decoupled, and the frictional forces were solved independently via trial-and-error algorithm. After that, the equations of motion were integrated numerically. Finally, two numerical examples were presented, and the results were compared with previous studies.

The methodology proposed in this paper can investigate the joint clearance as well as the deformation of the slider, and the statically indeterminate problem can be solved naturally. Different from KED method, the coupling between rigid body and flexible body motion can be taken into account, and the tedious judgements of contact modes between the slider and its guide is unnecessary. What's more, the precision and efficiency of this study are acceptable. Further studies could be done on rheonomic constraint between the slider and other bodies. If the slider have not only translational but also rotational motions, a floating frame of reference should be established.

Acknowledgements

This work is supported by a grant from National Natural Science Foundation of China (No. 11772021).

References

[1] Flores, P., Ambrósio, J., Claro, J.C.P., Lankarani, H.M.: Kinematics and dynamics of multibody systems with imperfect joints: Models and Case Studies. Spinger-Verlag, Berlin (2008)

[2] Flores, P.: Modeling and simulation of wear in revolute clearance joints in multibody systems. Mechanism & Machine Theory 44(6), 1211-1222 (2009).

[3] Flores, P., Koshy, C., Lankarani, H., Ambrósio, J., Claro, J.C.P.: Numerical and experimental investigation on multibody systems with revolute clearance joints. Nonlinear Dynamics 65(4), 383-398 (2011).

[4] Koshy, C.S., Flores, P., Lankarani, H.M.: Study of the effect of contact force model on the dynamic response of mechanical systems with dry clearance joints: computational and experimental approaches. Nonlinear Dynamics 73(1-2), 325-338 (2013).

[5] Marques, F., Flores, P., Claro, J.P., Lankarani, H.M.: A survey and comparison of several friction force models for dynamic analysis of multibody mechanical systems. Nonlinear Dynamics 86(3), 1407-1443 (2016).

[6] Marques, F., Isaac, F., Dourado, N., Souto, A.P., Flores, P., Lankarani, H.M.: A Study on the Dynamics of Spatial Mechanisms With Frictional Spherical Clearance Joints. Journal of Computational and Nonlinear Dynamics 12(5), 051013 (2017).

[7] Erkaya, S.: Experimental investigation of flexible connection and clearance joint effects on the vibration responses of mechanisms. Mechanism & Machine Theory 121, 515-529 (2018).

[8] Erkaya, S.: Clearance-induced vibration responses of mechanical systems: computational and experimental investigations. Journal of the Brazilian Society of Mechanical Sciences and Engineering 40(2), 90 (2018). doi:10.1007/s40430-018-1015-x

[9] Rahmanian, S., Ghazavi, M.R.: Bifurcation in planar slider–crank mechanism with revolute clearance joint. Mechanism and Machine Theory 91, 86-101 (2015).

[10] Farahan, S.B., Ghazavi, M.R., Rahmanian, S.: Nonlinear dynamic analysis of a four-bar mechanism having revolute joint with clearance. Journal of Theoretical and Applied Vibration and Acoustics 2(1), 91-106 (2016).

[11] Farahan, S.B., Ghazavi, M.R., Rahmanian, S.: Bifurcation in a planar four-bar mechanism with revolute clearance joint. Nonlinear Dynamics 87(2), 955-973 (2017).

[12] Tian, Q., Liu, C., Machado, M., Flores, P.: A new model for dry and lubricated cylindrical joints with clearance in spatial flexible multibody systems. Nonlinear Dynamics 64(1), 25-47 (2010).

[13] Tian, Q., Zhang, Y., Chen, L., Yang, J.: Simulation of planar flexible multibody systems with clearance and lubricated revolute joints. Nonlinear Dynamics 60(4), 489-511 (2010).

[14] Tian, Q., Liu, C., Machado, M., Flores, P.: A new model for dry and lubricated cylindrical joints with clearance in spatial flexible multibody systems. Nonlinear Dynamics 64(1), 25-47 (2011).

[15] Bai, Z.F., Jiang, X., Li, F., Zhao, J.J., Zhao, Y.: Reducing undesirable vibrations of planar linkage mechanism with joint clearance. Journal of Mechanical Science and Technology 32(2), 559-565 (2018). doi:10.1007/s12206-018-0103-7

[16] Bai, Z.F., Zhao, J.J., Chen, J., Zhao, Y.: Design optimization of dual-axis driving mechanism for satellite antenna with two planar revolute clearance joints. Acta Astronautica 144, 80-89 (2018).

[17] Muvengei, O., Kihiu, J., Ikua, B.: Dynamic analysis of planar multi-body systems with LuGre friction at differently located revolute clearance joints. Multibody System Dynamics 28(4), 369-393 (2012).

[18] Muvengei, O., Kihiu, J., Ikua, B.: Dynamic analysis of planar rigid-body mechanical systems with two-clearance revolute joints. Nonlinear Dynamics 73(1-2), 259-273 (2013).

[19] Muvengei, O., Kihiu, J., Ikua, B.: Dynamic Analysis of Multi-Body Mechanical Systems with Imperfect Kinematic Joints: A Literature Survey and Review. Sustainable Research & Innovation Proceedings 3 (2011).

[20] Tian, Q., Flores, P., Lankarani, H.M.: A comprehensive survey of the analytical, numerical and experimental methodologies for dynamics of multibody mechanical systems with clearance or imperfect joints. Mechanism and Machine Theory 122 (2018). doi:10.1016 j.mechmachtheory.2017.12.002

[21] Wilson, R., Fawcett, J.N.: Dynamics of the slider-crank mechanism with clearance in the sliding bearing. Mechanism and Machine Theory 9(1), 61-80 (1974). doi:10.1016/0094-114X(74)90008-1

[22] Farahanchi, F., Shaw, S.W.: Chaotic And Periodic Dynamics Of A Slider-Crank Mechanism With Slider Clearance. Journal of Sound & Vibration 177(3), 307-324 (1994).

[23] Klepp, H.J.: Modes of contact and uniqueness of solutions for systems with friction-affected sliders. Journal of Sound and Vibration 254(5), 987-996 (2002). doi:10.1006/jsvi.2001.4147

[24] Qi, Z., Luo, X., Huang, Z.: Frictional contact analysis of spatial prismatic joints in multibody systems. Multibody System Dynamics 26(4), 441-468 (2011). doi:10.1007/s11044-011-9264-9

[25] Flores, P., Ambrósio, J., Claro, J., Lankarani, H.: Translational joints with clearance in rigid multibody systems. Journal of Computational and Nonlinear Dynamics 3(1), 011007 (2008).

[26] Flores, P., Leine, R., Glocker, C.: Modeling and analysis of planar rigid multibody systems with translational clearance joints based on the non-smooth dynamics approach. Multibody System Dynamics 23(2), 165-190 (2010).

[27] Liu, C., Zhao, Z., Chen, B.: The bouncing motion appearing in a robotic system with unilateral constraint. Nonlinear Dynamics 49(1), 217-232 (2006).

[28] Zhao, Z., Liu, C., Chen, B.: The Painlevé paradox studied at a 3D slender rod. Multibody System Dynamics 19(4), 323-343 (2008).

[29] Wang, X., Lv, J.: Modeling and simulation of dynamics of a planar-motion rigid body with friction and surface contact. International Journal of Modern Physics B 31(16-19), 1744021 (2017).

[30] Acary, V.: Projected event-capturing time-stepping schemes for nonsmooth mechanical systems with unilateral contact and Coulomb's friction. Computer Methods in Applied Mechanics and Engineering 256, 224-250 (2013). doi:10.1016/j.cma.2012.12.012

[31] Chen, Q.Z., Acary, V., Virlez, G., Brüls, O.: A nonsmooth generalized - α scheme for flexible multibody systems with unilateral constraints. International Journal for Numerical Methods in Engineering 96(8), 487-511 (2013). doi:10.1002/nme.4563

[32] Zhuang, F., Wang, Q.: Modeling and simulation of the nonsmooth planar rigid multibody systems with frictional translational joints. Multibody System Dynamics 29(4), 403-423 (2013).

[33] Zhuang, F., Wang, Q.: Modeling and analysis of rigid multibody systems with driving constraints and frictional translation joints. Acta Mechanica Sinica 30(3), 437-446 (2014).

[34] Ting, K.-L., Hsu, K.-L., Yu, Z., Wang, J.: Clearance-induced output position uncertainty of planar linkages with revolute and prismatic joints. Mechanism and Machine Theory 111, 66-75 (2017). doi:10.1016/j.mechmachtheory.2016.09.012

[35] Zhang, J., Wang, Q.: Modeling and simulation of a frictional translational joint with a flexible slider and clearance. Multibody System Dynamics 38(4), 367-389 (2016). doi:10.1007/s11044-015-9474-7

[36] Wasfy, T.M., Noor, A.K.: Computational strategies for flexible multibody systems. Applied Mechanics Reviews 56(6), 553-613 (2003).

[37] Kerr, A.D.: Elastic and Viscoelastic Foundation Models. Journal of Applied Mechanics 31(3), 491-498 (1964). doi:10.1115/1.3629667

[38] Alves, J., Peixinho, N., da Silva, M.T., Flores, P., Lankarani, H.M.: A comparative study of the viscoelastic constitutive models for frictionless contact interfaces in solids. Mechanism and Machine Theory 85, 172-188 (2015). doi:10.1016/j.mechmachtheory.2014.11.020

[39] Xu, Z., Wang, Q., Wang, Q.: Numerical method for dynamics of multi-body systems with two-dimensional Coulomb dry friction and nonholonomic constraints. Applied Mathematics and Mechanics (English Edition) 38(12), 1733-1752 (2017).

[40] Fan, X., Walker, P.D., Wang, Q.: Modeling and simulation of longitudinal dynamics coupled with clutch engagement dynamics for ground vehicles. Multibody System Dynamics 43(2), 153-174 (2018).

[41] Pennestrì, E., Rossi, V., Salvini, P., Valentini, P.P.: Review and comparison of dry friction force models. Nonlinear dynamics 83(4), 1785-1801 (2016).

[42] Glocker, C.: Set-Valued Force Laws, Dynamics of Non-Smooth Systems, vol. 1. Lecture Notes in Applied Mechanics. Springer-Verlag Berlin Heidelberg, (2001)

[43] Bayo, E., Garcia De Jalon, J., Serna, M.A.: A modified lagrangian formulation for the dynamic analysis of constrained mechanical systems. Computer Methods in Applied Mechanics and Engineering 71(2), 183-195 (1988). doi:10.1016/0045-7825(88)90085-0

[44] Zienkiewicz, O.C., Taylor, R.L., Zhu, J.Z.: The Finite Element Method: Its Basis and Fundamentals. Butterworth-Heinemann (2013).

[45] Liu, L., Liu, H., Wu, Z., Yuan, D.: A new method for the determination of the zero velocity region of the Karnopp model based on the statistics theory. Mechanical Systems & Signal Processing 23(5), 1696-1703 (2009).